Brain Imaging and Behavior
DOI 10.1007/s11682-016-9528-3

ORIGINAL RESEARCH

"Small World" architecture in brain connectivity and hippocampal volume in Alzheimer's disease: a study via graph theory from EEG data

Fabrizio Vecchio[1] · Francesca Miraglia[1] · Francesca Piludu[2,3] · Giuseppe Granata[1] · Roberto Romanello[1] · Massimo Caulo[4] · Valeria Onofrj[3] · Placido Bramanti[2] · Cesare Colosimo[3] · Paolo Maria Rossini[1,5]

Abstract Brain imaging plays an important role in the study of Alzheimer's disease (AD), where atrophy has been found to occur in the hippocampal formation during the very early disease stages and to progress in parallel with the disease's evolution. The aim of the present study was to evaluate a possible correlation between "Small World" characteristics of the brain connectivity architecture—as extracted from EEG recordings—and hippocampal volume in AD patients. A dataset of 144 subjects, including 110 AD (MMSE 21.3) and 34 healthy Nold (MMSE 29.8) individuals, was evaluated. Weighted and undirected networks were built by the eLORETA solutions of the cortical sources' activities moving from EEG recordings. The evaluation of the hippocampal volume was carried out on a subgroup of 60 AD patients who received a high-resolution T1-weighted sequence and underwent processing for surface-based cortex reconstruction and volumetric segmentation using the Freesurfer image analysis software. Results showed that, quantitatively, more correlation was observed in the right hemisphere, but the same trend was seen in both hemispheres. Alpha band connectivity was negatively correlated, while slow (delta) and fast-frequency (beta, gamma) bands positively correlated with hippocampal volume. Namely, the larger the hippocampal volume, the lower the alpha and the higher the delta, beta, and gamma Small World characteristics of connectivity. Accordingly, the Small World connectivity pattern could represent a functional counterpart of structural hippocampal atrophying and related-network disconnection.

Highlights
- Functional connectivity and optimal network structure is essential for information processing in the brain.
- Progressive structural changes in the brain of Alzheimer Patients are associated with changes in connectivity and networks architecture.
- Aim of the present study was to correlate the network properties from EEG signals with hippocampal atrophy in cognitive decline patients (Alzheimer) by graph analysis tools.

Keywords Graph theory · Alzheimer · Functional connectivity · EEG · Hippocampus · eLORETA · MRI

✉ Fabrizio Vecchio
fabrizio.vecchio@uniroma1.it; fabrizio.vecchio@sanraffaele.it

[1] Brain Connectivity Laboratory, IRCCS San Raffaele Pisana, Via Val Cannuta, 247, 00166 Rome, Italy

[2] IRCCS Centro Neurolesi Bonino-Pulejo, Messina, Italy

[3] Department of Radiologic Sciences, Catholic University, Policlinic A. Gemelli, Rome, Italy

[4] Department of Neuorscience, Imaging and Clinical Sciences, University of Chieti, Chieti, Italy

[5] Department of Geriatrics, Neuroscience & Orthopedics, Institute of Neurology, Catholic University, Policlinic A. Gemelli, Rome, Italy

Introduction

Brain imaging has played a variety of roles in the study of Alzheimer's disease (AD) over the past four decades. Initially, computed tomography (CT) and then magnetic resonance imaging (MRI) were used diagnostically to rule out other causes of dementia, such as vascular or non-Alzheimer neurodegeneration, as well as reversible dementias. More recently, a variety of imaging modalities—including structural and functional MRI and positron emission tomography (PET) studies of cerebral metabolism and amyloid plaque tracers via specific radioligands—have shown characteristic changes in the brains of AD patients. Changes also appear in the prodromal and presymptomatic stages, making it easier to rule in/out the AD pathophysiological process.

Published online: 09 March 2016

Increasing evidence from structural and functional MRI studies suggests that Alzheimer's disease and mild cognitive impairment may target specific brain networks (deToledo-Morrell et al. 2004). Structural imaging can detect the time course of brain atrophying in patients with Alzheimer's disease and may serve as a surrogate marker for pathological changes in people suspected of having AD.

In broad terms, structural MRI in AD can be utilized to assess atrophy (or volumes) and changes in tissue characteristics. These cause signal alterations to certain sequences—such as white matter hyperintensities—on the T2-weighted MRI, as a result of gliotic lesions secondary to vascular damage. A number of MR sequences that are sensitive to microstructural change (e.g., magnetization transfer or diffusion) have shown alterations in AD. Volumetric MRI is becoming an increasingly important tool in the early detection and care of people suspected of having mild cognitive impairment or Alzheimer's disease (Scheltens et al. 2002).

MRI–based measures of atrophy are regarded as valid markers of a disease's state and progression for several reasons (Marizzoni et al. 2015). Progressive atrophy is considered a counterpart of concomitant neurodegeneration and disease evolution in cognitive decline. Moreover, the topography of brain tissue loss correlates with cognitive deficits, both cross-sectionally and longitudinally. Patients with Alzheimer's disease may express typical pathologic changes in cortical gray matter, characterized by the accumulation of amyloid beta plaques, the formation of neurofibrillary tangles, and neuronal and synaptic loss (Delacourte et al. 1999). All these changes lead to cerebral atrophy in specific brain regions and networks. The pattern of neuronal/synaptic depauperation differs across various forms of dementia, reflecting selective vulnerability and/or regional disease expression, and it is becoming increasingly clear that—by the time a typical AD patient receives a diagnosis—regions within his or her brain have already been atrophying for several years, well before symptom onset. This is partially contrasted by the neural/synaptic reserve and plasticity (see for a review D'Amelio and Rossini 2012). In patients with Alzheimer's disease, atrophy has been found to occur in the hippocampal formation and entorhinal cortex, as has been demonstrated by several volumetric MRI studies (Apostolova et al. 2012; Du et al. 2001; Killiany et al. 2002; Wolz et al. 2011; Zimny et al. 2011). Actually, the vast majority of structural brain imaging studies have been based on histopathological evidence that the entorhinal cortex and hippocampus are among the first sites impacted by the disease during its pre-symptomatic stages, including Mild Cognitive Impairment (MCI).

Among the different MRI markers of AD (Modrego 2006), the rate of whole-brain and hippocampal atrophy, as assessed on high-resolution T1-weighted MRI, is well established and validated, and is increasingly being used as an outcome measure in clinical trials experimenting with potentially disease-modifying therapies. Recently, three-dimensional gradient-echo sequences have allowed for the calculation of volumes and the co-registration of images during the follow-up phase and have been used in clinical practice (Whitwell et al. 2001). Despite their convoluted structure, the boundaries of the hippocampal formation (and adjacent CSF spaces) are easier for human operators or automated algorithms to recognize than the amygdala, entorhinal cortex, or parahippocampal gyrus. This is because the anatomical boundaries of the hippocampus are distinct on high-resolution T1-weighted MRI scans around most of the surface of the structure.

Unlike T1-weighted imaging, T2 relaxometry allows for the quantitative measurement of signal changes on T2-weighted images. However, the ability of T2-weighted imaging to differentiate MCI from AD and Nold is limited, because various confounding pathologies—such as brain edema, demyelination, and axonal loss—may also result in changes similar to those seen in Alzheimer's disease. Early reports used serial manual detection of the anatomical boundaries of the hippocampus and entorhinal cortex (Pitkanen et al. 1996). Hippocampal volume measured in vivo by MRI correlates with the Braak stage and neuronal counts (Bobinski et al. 2000; Gosche et al. 2002; Jack et al. 2002). Patients with MCI have a smaller entorhinal cortex and hippocampus than healthy age-matched subjects. However, patients with AD may experience a prominent volume reduction in the entorhinal cortex and hippocampus. During the mild AD stage, hippocampal volume is already reduced by 15–30 % relative to controls (van der Flier et al. 2005), and in the amnestic variant of MCI the volume is reduced by 10–15 % (Barnes et al. 2007; Shi et al. 2009). Furthermore, new Alzheimer's disease criteria allow for an earlier diagnosis of the disease by including biomarkers derived from cerebrospinal fluid or hippocampal volume analysis (Dubois et al. 2010; Dubois et al. 2014). Altogether, structural MRIs can help support a clinical diagnosis, but unfortunately such techniques are not sufficient to establish a definitive diagnosis, as often the overlap between atrophy associated with "healthy aging" and AD is too great.

Characteristics of neural firing synchronization of the oscillating rhythms in resting eyes-closed electroencephalographic (EEG) recordings have been repeatedly demonstrated to become abnormal during the pre-clinical and clinical AD stages (Vecchio et al. 2015a; Vecchio et al. 2014b). Moreover, it was demonstrated that a network analysis of the EEG recordings could improve the discrimination of AD, and that this analysis could correlate with the structural brain data revealed by DTI (Vecchio et al. 2015a; Vecchio et al. 2014b).

Network connectivity properties were usually quantified in the framework of graph formalism by means of Clustering Coefficient (C) and Path Length (L) (Miraglia et al. 2015a; Stam et al. 2009; Stam et al. 2007; Vecchio et al. 2014a, b), which also deal with the "small world" properties of networks in AD. In Stam et al. 2007, no changes of C or increases of L

were reported in AD. A decrease of C and L for the AD condition was found in Stam et al. 2009, which was interpreted as a loss of resting state connectivity and a tendency to a more random networks. Regarding this kind of functional network analysis, Watts and Strogatz introduced the concept of 'small-world' networks, allowing for an optimal balance between local specialization (C) and global integration (L) (Watts and Strogatz 1998). This approach, combined with graph theory concepts, is a promising way to characterize brain functional organization (Bassett and Bullmore 2006); it correlates with behavioral and clinical, as well as structural, findings. It also allows researchers to evaluate whether the functional connectivity patterns between brain areas reproduce the organization of more or less strongly connected networks based on the time-varying strength of synchronization in the oscillatory neuronal firings of brain regions representing the network's nodes (Vecchio et al. 2014a; Vecchio et al. 2015b; Vecchio et al. 2014b, c).

Within this theoretical frame, our working hypothesis was that hippocampal atrophy and the functional network of the cortical sources in resting EEG rhythms could be inter-related. Consequently, the aim of this study was to determine whether the "Small World" connectivity characteristic (as the ratio between Clustering and Path Length, namely the evaluation of this optimal balance between local specialization and global integration) of the resting state brain networks correlated with hippocampal atrophy in subjects affected by Alzheimer's Disease.

Subjects and methods

Participants

A dataset of 144 EEG recordings was analyzed. The patient group included 110 AD (MMSE 21.3), while the control group included 34 healthy subjects Nold (MMSE 29.8). The mean age was about 74 years across the two groups. Part of the present dataset (healthy subjects) was previously used for other studies (Miraglia et al. 2015a; Vecchio et al. 2016). Demographic data are reported in Table 1.

All subjects were right-handed, according to the Handedness Questionnaire. Informed consent was obtained from each subject, and the study was approved by the local ethical committee. Experimental procedures conformed to the Declaration of Helsinski and national guidelines.

Table 1 Demographic data of the partecipants

	Age (years)	Gender	Education (years)	MMSE
Nold	73.2 ± 0.5	80 F	7 ± 0.4	21.3 ± 0.3
AD	73.8 ± 0.7	20 F	8 ± 0.9	29.8 ± 0.3

Inclusion and exclusion criteria

All subjects took part in a battery of neuropsychological tests that assessed their attention, memory, executive function, visuo-construction abilities, and language. Memory was assessed by means of the immediate and delayed recall of the Rey Auditory Verbal Learning Test (Carlesimo et al. 1996), the delayed recall of Rey figures (Rey 1968), the delayed recall of a three-word list (Chandler et al. 2004), the delayed recall of a story, and a short-term memory performance assessed via digit span for both forward and backward tasks (Monaco et al. 2013). Pathological performances on memory tasks were set below the 5th percentile of the normal population.

Each subject was also examined by expert neurologists and submitted to a list of diagnostic tests, including the MRI, SPECT (Single Photon emission Tomography), MMSE (Mini-Mental State Evaluation), clinical dementia rating (Hughes et al. 1982), geriatric dementia score (GDS; (Yesavage et al. 1982)), Hachinski Ischemic Score (HIS; (Rosen et al. 1980)), and Instrumental Activities of Daily Living scale (IADL; (Lawton and Brody 1969)) to confirm the diagnosis and to exclude other causes of dementia, such as frontotemporal dementia, vascular dementia, extrapyramidal syndromes, reversible dementias, and Lewy body dementia. When required, a lumbar puncture was carried out to measure A-Beta and Tau protein contents.

AD was diagnosed according to the National Institute on Aging-Alzheimer's Association workgroups (McKhann et al. 2011) and DSM IV TR criteria. Exclusion criteria for AD included any evidence of (i) frontotemporal dementia, (ii) behavioural variants of frontotemporal dementia, (iii) vascular dementia, (iv) extra-pyramidal syndromes, (v) reversible dementias (including the pseudodementia of depression); and (vi) Lewy body dementia.

Clinical diagnosis was corroborated by the presence of a significant reduction in hippocampal volume, increased width of the temporal horn, and an increase of the choroidal fissure of between 2 and 4 on the likeart scale in MRI (Roman et al. 1993).

Data recordings and preprocessing

The EEG recording was performed at rest, with closed eyes and no task conditions (for at least 5 min), while the subject was seated and relaxed in a sound-attenuated and dimly lit room, or in bed. Electroencephalographic signals were measured from 19 electrodes (Fp1, Fp2, F7, F8, F3, F4, T3, T4, C3, C4, T5, T6, P3, P4, O1, O2, Fz, Cz and Pz) positioned according to the International 10–20 system (linked ears reference). The monitoring of the eye movements was obtained from two different channels: vertical and horizontal EOGs. Skin/electrode impedances were lowered below 5 KΩ.

Data were analyzed with Matlab R2011b software (Math Works, Natick, MA) using scripts based on the EEGLAB 11.0.5.4b toolbox (Swartz Center for Computational Neurosciences, La Jolla, CA; www.sccn.ucsd.edu/eeglab). The EEG recordings were band-pass filtered from 0.2 to 47 Hz using a finite-impulse response (FIR) filter, and the sampling rate frequency was set up at 256 Hz. To eliminate interference caused by ocular, muscular, cardiac, and other types of artifacts, imported data were fragmented in 2 s duration epochs and used for two processes. The data were reviewed, and the epochs with aberrant waveforms or with evident epileptiform activity were manually discarded by an expert EEGer. Second, artifact detection/rejection was completed through independent component analysis (ICA) using the Infomax ICA algorithm, as implemented in the EEGLAB. ICA is a blind source decomposition algorithm that enables the separation of statistically independent sources from multichannel data. It effectively separates ocular movements and blink artifacts from EEG data (Iriarte et al. 2003; Jung et al. 2000). The components were then visually inspected, and, if artifact contamination was found, they were manually rejected.

Functional connectivity analysis

EEG functional connectivity analysis has been performed using low resolution electromagnetic tomography software to compute the cortical three-dimensional distribution of the current density (Miraglia et al. 2015a, b; Vecchio et al. 2014a, b, c): free academic software is publically available at http://www.uzh.ch/keyinst/NewLORETA/LORETA01.htm). The eLORETA algorithm is a linear inverse solution for EEG signals. Because it has no localization error, it points to sources under ideal (noise-free) conditions (Pascual-Marqui 2002).

The eLORETA method is a discrete, three-dimensionally (3D) distributed linear, weighted minimum-norm inverse solution. The particular weights used endow the tomography with the property of exact localization to test point sources, yielding images of current density with exact localization, albeit with low spatial resolution (i.e. neighboring neuronal sources will be highly correlated). The description of the method and the proof of its exact zero-error localization property are described in Pascual-Marqui 2009. It is also important to emphasize that eLORETA has no localization bias, even in the presence of structured noise. It should further be emphasized that the localization properties of any linear 3D-inverse solution (i.e. tomography) can always be determined by localization errors to test point sources. If such a tomography has zero localization error to such point sources located anywhere in the brain, then—except in the case of low spatial resolution—the tomography will correctly localize any arbitrary 3D distribution. This is due to the principles of linearity and superposition.

The previously developed, related tomography, LORETA (Pascual-Marqui et al. 1994), has received considerable validation from studies combining LORETA with other more established localization methods, such as fMRI (Mulert et al. 2004; Vitacco et al. 2002), structural MRI (Worrell et al. 2000), and PET (Dierks et al. 2000; Pizzagalli et al. 2004; Zumsteg et al. 2005). Further, LORETA validation has been based on accepting as a ground truth the localization findings obtained from invasive, implanted depth electrodes. Pertinently, there are several studies in epilepsy (Volpe et al. 2007; Zumsteg et al. 2006a, b, c) and cognitive ERPs (Pizzagalli et al. 2001). Furthermore, sLORETA (Pascual-Marqui 2002) has recently been validated in several simultaneous EEG/fMRI studies (Mobascher et al. 2009; Olbrich et al. 2009), and in an EEG localization study for epilepsy (Rullmann et al. 2009). All these results validate the accuracy measure of the eLORETA method, which is also supported by several EEG/fMRI studies (Mobascher et al. 2009; Olbrich et al. 2009), and in an EEG localization study for epilepsy (Rullmann et al. 2009), due to its improved localization properties. Others (Greenblatt et al. 2005; Sekihara et al. 2005) showed that the method has a high degree of accuracy and no localization bias in the absence of measurement noise; however, in the presence of measurement noise they found that sLORETA has a localization bias. Furthermore, several recent studies from independent groups (Aoki et al. 2015; Barry et al. 2014; Canuet et al. 2011; Ikeda et al. 2015; Ramyead et al. 2014; Vecchio et al. 2014a; Vecchio et al. 2015a; Vecchio et al. 2014b; Vecchio et al. 2016) supported correct source localization using eLORETA, along with a 19-electrode EEG recording with a standard 10–20 montage.

For the current implementation of eLORETA, computations were made for a realistic head model (Fuchs et al. 2002) using the MNI152 template (Mazziotta et al. 2001), with the three-dimensional solution space restricted to cortical gray matter, as determined by the probabilistic Talairach atlas (Lancaster et al. 2000). The standard electrode positions on the MNI152 scalp were taken from Jurcak et al. 2007. The intracerebral volume was partitioned in 6239 voxels at a 5 mm spatial resolution. Thus, eLORETA images represented the electric activity at each voxel in the neuroanatomic Montreal Neurological Institute (MNI) space as the exact magnitude of the estimated current density. Anatomical labels—such as Brodmann areas—are also reported using MNI space, corrected to Talairach space (Brett et al. 2002).

To obtain a topographic view of the whole brain, brain connectivity was computed with sLORETA/eLORETA software in 84 regions, positioning the center in the available 42 Brodmann Areas (BAs: 1, 2, 3, 4, 5, 6, 7, 8, 9, 10, 11, 13, 17, 18, 19, 20, 21, 22, 23, 24, 25, 27, 28, 29, 30, 31, 32, 33, 34, 35, 36, 37, 38, 39, 40, 41, 42, 43, 44, 45, 46, 47) in the left and right hemispheres.

Regions of Interest (ROIs) are needed to estimate the electric neuronal activity used to analyze brain functional connectivity. No general rules for constructing the ROIs are available. The signal at each cortical ROI consisted of the average electric neuronal activities of all voxels belonging to that ROI, as computed with eLORETA.

For each hemisphere, among the eLORETA current density time series of the 42 ROIs, intracortical Lagged Linear Coherence, extracted using a sphere with a 19-mm radius (Pascual-Marqui 2007), was computed between all possible pairs of the ROIs for each of the five independent EEG frequency bands of delta (2–4 Hz), theta (4–8 Hz), alpha 1 (8–10.5 Hz), alpha 2 (10.5–13 Hz), beta 1 (13–20 Hz), beta 2 (20–30 Hz), and gamma (30–45 Hz) for each subject.

The well-known definition for the complex valued coherence between time series x and y in the frequency band ω is:

$$r_{xyw} = \frac{ReCov(x,y) + iImCov(x,y)}{\sqrt{Var(x)*Var(y)}} \quad (1)$$

which is based on the cross-spectrum given by the covariance andvariances of the signals, where i is the imaginary unit ($\sqrt{-1}$).

Beginning with the definition of the complex valued coherence between time series x and y in the frequency band ω—which is based on the cross-spectrum given by the covariance and variances of the signals—the lagged linear coherence in the frequency band ω is reported in acordance with the following equation (Pascual-Marqui 2007):

$$LagR^2_{xyw} = \frac{[ImCov(x,y)]^2}{Var(x)*Var(y) - [ReCov(x,y)]^2} \quad (2)$$

Where *Var* and *Cov* are variances and covariances of the signals.

It was developed as a measure of true physiological connectivity not affected by volume conduction and low spatial resolution (Pascual-Marqui 2007). The values of lagged linear connectivity computing between all pairs of ROIs for each frequency band were used as weights of the networks built in the graph analysis.

A weighted network was built based on the connectivity between ROIs. The nodes of the network are ROIs, and the edges of the network are weighed by the lagged linear coherence values.

Graph analysis

A network is a mathematical representation of a real-world complex system. It is defined by a collection of nodes (vertices) and links (edges) between pairs of nodes. Nodes in large-scale brain networks usually represent brain regions, while links represent anatomical, functional, or effective connections (Friston 1994), depending on the dataset. Anatomical connections typically correspond to white matter fiber tracts between pairs of grey matter brain regions (cortical areas or subcortical relays). Functional connections correspond to magnitudes of temporal correlations in activity and may occur between pairs of anatomically unconnected regions.

A weighted graph is a mathematical representation of a set of elements (vertices) that may be linked through connections of variable weights (edges).

In the present study, weighted and undirected networks were built. The vertices of the networks are the estimated cortical sources in the BAs, and the edges are weighted by the Lagged Linear value within each pair of vertices. The software instrument used here for the graph analysis was the Brain Connectivity Toolbox (BCT, http://www.brain-connectivity-toolbox.net/), adapted with our own Matlab scripts.

The clustering (C) around vertex i is quantified by the number of triangles in which vertex i participates, normalized by the maximum possible number of such triangles. This quantity is normalized between 0 and 1, and it characterizes the tendency of the nearest neighbors of node i to be interconnected. As triangles are one type of subgraph, the definition of C may be used to yield the weighted Clustering coefficient C^w by replacing the number of triangles *ti* with the sum of triangle intensities (Onnela et al. 2005).

The mean clustering coefficient is computed for all nodes of the graph and is then averaged. It represents the tendency of a network's elements to form local clusters.

Weighted Characteristic Path length L^w is defined by Onnela et al. 2005; it represents the shortest weighted path length between i and j. f is a map (e.g., an inverse) from weight to length, and $gi^w \leftrightarrow j$ is the shortest weighted path between i and j. To obtain individual normalized relative measures, the values of the characteristic path length and of the clustering coefficient were divided by the mean values obtained by the average of themselves in the bands of each subject.

The Small-world property was evaluated as the ratio between relative Clustering and Path Length measure for each subject.

Structural MRI acquisition parameters and image processing

All subjects received a diagnostic MRI study on 1.5 T GE Health Care and Siemens MRI scanners to ascertain brain pathology. Small vessel disease was identified on MRI as silent lacunar infarcts (small hypointense -CSF isointense-regions on T1-weighted MRI), or as white matter hyperintensities that appear to punctuate or diffuse regions of hyperintense signal on T2 and FLAIR MRI, or micro bleeds on the gradient echo (T2*) MRI.

Sixty out of the 110 patients with Alzheimer's disease also received also a morphometric MRI study that had to include one high-quality and high-resolution T1-weighted sequence.

According to standardized ADNI protocol (Jack et al. 2008) options for this high-quality 3D T1-weighted sequence were a magnetization prepared rapid gradient echo (MP-RAGE) with the following parameters: a repetition time (TR) of 2400 ms; a minimum full TE, inversion time (TI) of 1000 ms, a flip angle of 8°; and a voxel size with a 1.0 mm slice thickness, with no gaps.

The quality of the structural high-resolution structural brain MRI scans were rated by two experienced neuroimaging researchers (FP and MC) according to a three-point rating scale: 0 = no motion artifacts, excellent quality; 1 = a few motion artifacts, fair quality; and 2 = moderate/severe motion artifacts, poor quality. Only datasets with scores of 0 were considered to be of sufficient quality for research purposes. The criteria used to define quality were (a) signal-to-noise ratio; (b) tissue contrast; and (c) artifacts, including c1) motion artifacts (ghosting and smearing); c2) edge artifacts (ghosting, chemical shifts, and ringing); c3) distortions; and c4) aliasing (wrap-around) artifacts.

The neuroradiologists were blinded to all clinical data and diagnostic categories. The raw 3D T1 MRI data gleaned from sixty patients underwent processing for surface-based cortex reconstruction and volumetric segmentation using the Freesurfer image analysis software (version 5.3.0), which is documented and freely available for download online (http://surfer.nmr.mgh.harvard.edu/) and can be installed on a OSX Mavericks 10.9.3.

All subjects were affine-registered to the Talairach atlas (Fox et al. 1996). Image intensity variations due to magnetic fields in homogeneities were normalized. Then a skull stripping algorithm was applied and the non-brain tissue was removed using a hybrid watershed/surface deformation procedure (Fox et al. 2001). Hereafter, cutting planes were used to separate the hemispheres, cerebellum, and brain stem.

Next, an estimate of the gray/white boundary was constructed by classifying all white matter voxels in an MRI volume. The surface of the white matter voxels was refined to obtain better accuracy in the gray/white boundary and was then subsequently deformed outward to find the pial surface, according to Fischl and Dale (Jack et al. 1999). The surface deformation was based on a local adaptive estimation of the MRI values at the different surfaces by minimizing a constrained energy function. Cortical and subcortical labeling was performed utilizing a transformation that maps the individual subjects into a probabilistic atlas.

Image outputs from each stage of the Freesurfer processing were visually inspected and, if necessary, edited by the imaging analysts (FP and MC) to refine the segmentation and correct software delineation errors. For subsequent analyses among patients and control subjects, hippocampal measurements were normalized to the hemispherical grey matter cortex.

Statistical evaluation

The eLORETA statistical evaluation was made with a graph analysis pattern extracted through sLORETA/eLORETA from the brain network (including 42 ROIs in the left and 42 ROIs in the right hemisphere). The normality of the data was tested using the Kolmogorov-Smirnov test, and the hypothesis of Gaussianity could not be rejected. In order to confirm the goodness of the data, a statistical ANOVA design was addressed for the Small World among the factors' Side (left and right hemisphere), Group (AD, Nold), and Band (delta, theta, alpha 1, alpha 2, beta 1, beta 2, gamma). Furthermore, a statistical t test was also administered for the normalized hippocampal volume in the two hemispheres.

Finally, for each hemisphere, Pearson's linear correlations were tested between the Small-world coefficient in each frequency band and the normalized hippocampal volume in the Alzheimer sub-group (Bonferroni corrected to obtain $p < 0.05$).

Results

Figure 1 illustrates the connectivity patterns of the eLORETA connectivity maps for the two groups of subjects in the explored frequencies. The maps illustrated only the connections (among the 84 ROIs mentioned: 42 left and 42 right BAs) that resulted in a higher than arbitrary threshold for each frequency band. The arbitrary threshold was selected through visual inspection in order to show the differences among groups. No statistical analysis was evaluated regarding the functional connection in the groups, as the aim of the present study was to test the variation of graph pattern and not single connections. Visual inspection shows that AD subjects present a higher number of connections in the lower frequency bands than Nold. Moreover, alpha bands present a focal localization in the posterior areas that decreases the number of tracts in AD with respect to the Nold group.

ANOVA findings suggests that Small World characteristics statistically interacted ($F(6852) = 5.64$; $p < 0.00001$) between the factors Group (AD, Nold) and Band (delta, theta, alpha 1, alpha 2, beta 1, beta 2, gamma; Fig. 2). Duncan planned post-hoc testing showed that, in line with previous evidence (Miraglia et al. 2015a; Vecchio et al. 2016), Nold presented higher Small World values than AD in the delta, theta, and beta bands ($p < 0.05$), while the opposite was found in the alpha bands, for which Nold presented lower values with respect to AD ($p < 0.05$).

Structural MRI analysis of normalized hippocampal volume showed no significant statistical t test between the two hemispheres ($p > 0.8$).

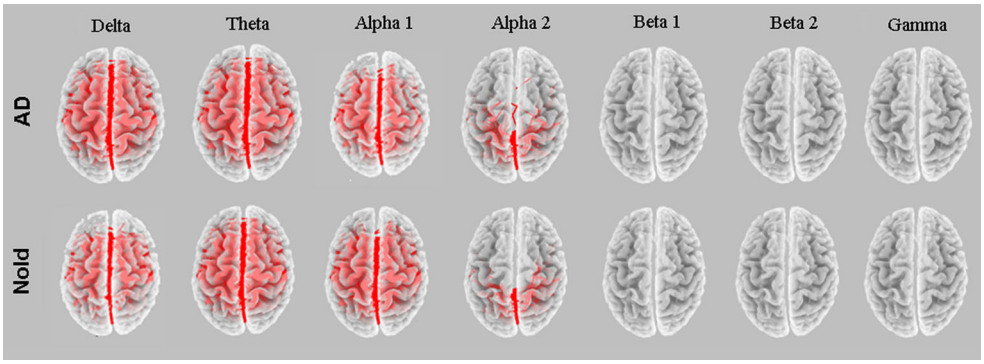

Fig. 1 Small World trends in the two groups of subjects

Correlation analysis in the AD group was performed among the weighted Small World coefficients in all seven bands and the normalized hippocampal volume. All significant comparisons are reported in Table 2. In summary, left hemisphere Small World coefficients positively correlate with the normalized volume of the left hippocampus in the beta 2 band and negatively in the alpha 1 band. In the right hemisphere, Small World coefficients positively correlate with the normalized volume of the right hippocampus in the delta, beta 2, and gamma bands, and negatively in the alpha bands. Figure 3 reports the scatterplots of these two correlations.

Discussion

The human brain consists of a complex network of inhibitory and excitatory circuits linking functionally specialized areas in a continuous, time-varying interplay—within a temporal frame of milliseconds—to acquire, share and integrate information in a constant state of dynamic fluctuations also governed by a number of variables including attention, emotions, motivation, arousal which finally influence network performance. Functional brain abnormalities are invariably reflected in changes of connectivity and networks architecture.

White-matter (axonal) fibers provide an anatomical basis for signal transfer and communication; these connections are not random, but are organized in a "small-world" network architecture characterized by a high degree of local clustering (segregation) and the presence of long-distance connections (integration). A well-designed anatomical network could combine the occurrence of functionally specialized (segregated) modules with a robust number of intermodular (integrating) links. Such a design is commonly termed Small-World and indeed appears to be a ubiquitous facet of anatomical connectivity. It is commonly thought that such an organization reflects an optimal balance of functional integration and segregation (Sporns and Honey 2006). Many studies investigated the topological changes of brain networks with different modalities, including structural MRI, diffusion tensor imaging in MRI, EEG/MEG, and fMRI (recently reviewed by Jovicich et al. 2015; Xie and He 2011). Therefore, Alzheimer's disease brain functional topography can be represented by a progressive derangement of network organization in hub regions and long-range connections causing small-world architecture alterations (Vecchio et al. 2015b).

Within this frame, the present study demonstrated that resting state Small World characteristics in several EEG frequency bands correlate with hippocampal volume. It is concluded that such a Small World pattern might represent a functional counterpart of structural brain modifications in AD. In fact, the aim of the present study was to evaluate a possible correlation between Small World characteristics of brain connectivity and hippocampal volume. Results show that quantitatively more correlations were observed in the right hemisphere, but with the some trend in both hemispheres. In particular, alpha bands were negatively correlated, while low and

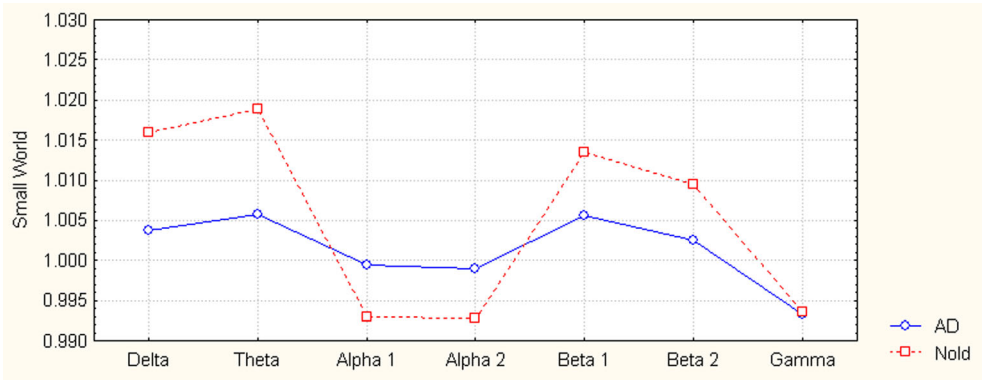

Fig. 2 Small World trends in the two groups of subjects

Table 2 Correlation analysis in performed among the weighted Small World coefficient in all seven bands and the normalized hippocampal volume. All significant comparisons are reported

	Left	Right
Delta		$r = 0.2626$; $p = 0.0409$
Theta		
Alpha 1	$r = -0.2492$; $p = 0.0508$	$r = -0.2505$; $p = 0.0515$
Alpha 2		$r = -0.2702$; $p = 0.0352$
Beta 1		
Beta 2	$r = 0.2925$; $p = 0.0211$	$r = 0.3742$; $p = 0.0030$
Gamma		$r = 0.3804$; $p = 0.0025$

high frequency bands (delta, beta, gamma) were positively correlated with the hippocampal volume. Specifically, the larger the hippocampal formation, the lower alpha and the higher the delta, beta, and gamma Small World architecture.

In line with previous evidence, it is clear that a reduction in the hippocampal volume leads to less Small World variability in the different EEG frequency bands. It was already demonstrated (Vecchio et al. 2015b)—and has been hereby replicated—that significant small-worldness difference distinguish normal elderly subjects from AD patients; for instance it is hereby confirmed that normal aging presents a higher specialization of Small World band characteristics with higher values in lower frequencies and lower values in alpha bands. Here, correlation analysis has shown that the reduction of hippocampal volume is combined to a loss in the Small World specialization in the EEG frequency bands. In other words, the Small World could present less of a spread of values. The present results provide a preliminary view on these relationships and should be taken into account also for other kinds of dementia or mild cognitive impairment in order to understand the effect of hippocampal volume in absence of overt dementia.

Of note, regarding the possibility of a bias due to the common feeding effect described in previous literature (Blinowska and Kaminski 2013; Kaminski et al. 1997), the methods used in the present work tried to avoid the bias of more connections in specific brain regions (explained by common feeding from electrodes generating a multitude of false connections between electrodes; Blinowska and Kaminski 2013); it is well-known that—for instance—the sources in the resting state eyes closed EEG are located in the posterior regions of the brain, with smaller contributions to frontal areas, therefore implementing a weighted graph for the proposed analyses and avoiding an aggregation of connection in spotted brain regions while considering all the possible connections with weight.

Furthermore, as a general limitation of the present study, it the low number of EEG channels should be considered. It was also reported that many studies used the same number of electrodes, but a replication of the present study with a large number of electrode derivations should be provided. Meanwhile, findings with a standard number of EEG recording channels—as used in routine clinical activity—are encouraging for large-scale future clinical applications.

Some points need to be discussed more specifically. The first is the functional relationships between hippocampal volume and cortical sources regarding the network of delta and alpha rhythms. Cholinergic basal forebrain neurons of medial septum heavily project to the hippocampus and the amygdala, which are connected to the cortical mantle by abundant non-cholinergic projections (Selden et al. 1998). These cholinergic pathways would drive cortico-cortical and thalamocortical loops to converge to cortical pyramidal neurons that generate low-band (8–10.5 Hz) alpha EEG oscillations, representing the dominant rhythms of the human brain in waking rest (Klimesch 1996, 1997; Steriade and Llinas 1988) (Klimesch et al. 1998; Ricceri et al. 2004; Rossini et al. 1991). To support this view, it has been reported that the cholinergic basal forebrain was more structurally impaired in AD patients (Teipel et al. 2005), especially in non-responders to cholinergic therapy (Tanaka et al. 2003). Finally, alpha and delta rhythms were found to be abnormally modulated in AD patients, as a function of disease severity and in opposite ways (see Vecchio et al. 2013). In particular, posterior cortical alpha rhythms were correlated with hippocampal volume (Babiloni et al. 2009). The complex interaction of the aforementioned factors accounts for the present finding of correlations between normalized hippocampal volume and the organization of the cortical delta and alpha source networks, as revealed by Small World characteristics.

A second main observation is that hippocampal atrophy was not significantly correlated to cortical source networks of EEG theta rhythms. It has been revealed that theta rhythms functionally connect the hippocampal/amygdala systems and the cortex (Buzsaki and Draguhn 2004; Selden et al. 1998). Moreover, cholinergic projection into the hippocampus regulates the hippocampal theta rhythms (Andersen et al. 2007; Kimura 2000). Accordingly, it can be speculated that hippocampal volume would not affect interactions between the basal forebrain pathways projecting to the hippocampus/amygdala and those directly projecting to the cerebral cortex (mainly modulated by alpha rhythms). Thus, the theta rhythms that modulate the cortical networks are mainly maintained with respect to the hippocampal volume, at least at the considered level of atrophy.

Finally, the correlation of the high frequency bands (beta and gamma) builds upon previous evidence of a similar correlation between gamma Small World reduction and memory decline, as revealed by specific memory tests (Vecchio et al. 2016). Despite a general acceptance of the idea that memory is not localized to one specific neural structure, there is overwhelming evidence that the medial temporal lobe (MTL), and particularly the hippocampal relays, play a central role in memory performance, via interactions with distributed

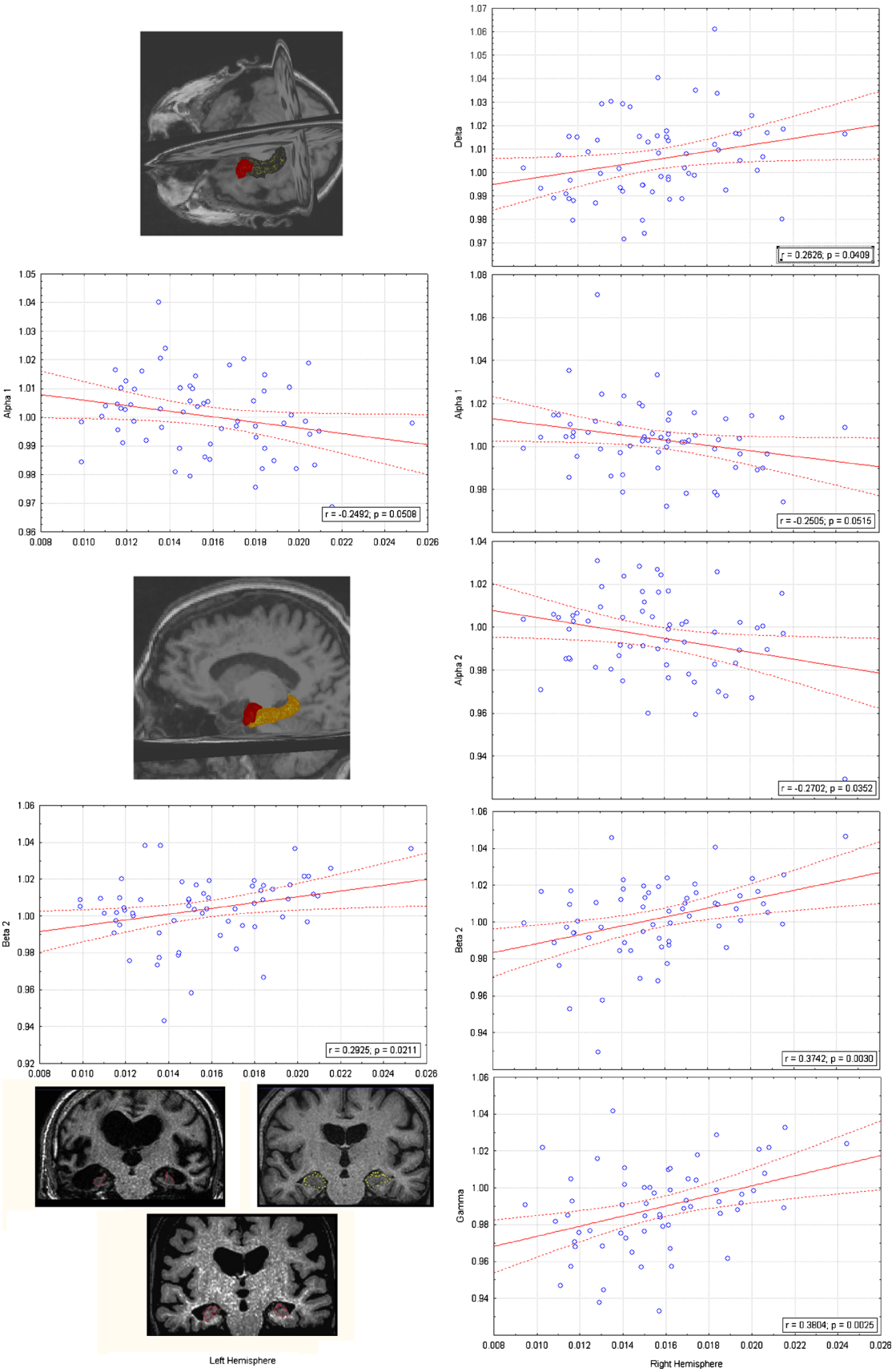

Fig. 3 Scatterplots of Small World correlation with hippocampal volume

cortical regions (Pohlack et al. 2014; Rienstra 2013; Scoville and Milner 1957). Here, moving from the idea that any normal-sized structure will support normal function and vice-versa (Van 2004), it is possible to speculate that the atrophy of the hippocampus could lead to memory impairment through the modulation of high-frequency Small World characteristics.

Conclusions

Understanding the role EEG oscillations play in the network dynamics of AD patients is important for comprehending mechanisms of cognitive decline and could serve as a model for understanding large-scale brain network dynamics and their relation to other cognitive phenomena or structural modulations. The hippocampal atrophy comes along with the background histo-pathophysiological alterations of AD. All these signs of neurodegeneration are mirrored by the small-world disorganization and lead to the cognitive impairment that has been clinically assessed. This study opens interesting avenues into future researches investigating eventual modifications of brain connectivity in the evolution of neurodegenerative processes beginning at the very early, pre-clinical stages.

Acknowledgments Dr. Francesca Miraglia participated to this study in the framework of her Ph.D. program at the Doctoral School in Neuroscience, Department of Neuroscience, Catholic University of Rome, Italy. This work was supported by the Italian Ministry of Health for Institutional Research (Ricerca corrente) and by the Italian Ministry of Instruction, University and Research MIUR ("Approccio integrato clinico e sperimentale allo studio dell'invecchiamento cerebrale e delle malattie neurodegenerative: basi molecolari, epidemiologia genetica, neuroimaging multimodale e farmacogenetica. (Merit)" and "Functional connectivity and neuroplasticity in physiological and pathological aging. Prot. 2010SH7H3F (ConnAge)" PRIN project).

Compliance with ethical standards

Funding This work was supported by the Italian Ministry of Health for Institutional Research (Ricerca corrente) and by the Italian Ministry of Instruction, University and Research MIUR ("Approccio integrato clinico e sperimentale allo studio dell'invecchiamento cerebrale e delle malattie neurodegenerative: basi molecolari, epidemiologia genetica, neuroimaging multimodale e farmacogenetica. (Merit)" and "Functional connectivity and neuroplasticity in physiological and pathological aging. Prot. 2010SH7H3F (ConnAge)" PRIN project).

Conflict of interest All authors declare that they have no conflict of interest.

Ethical approval All procedures performed in studies involving human participants were in accordance with the ethical standards of the institutional and/or national research committee and with the 1964 Helsinki declaration and its later amendments or comparable ethical standards.

Informed consent Informed consent was obtained from all individual participants included in the study.

References

Andersen, P., Morris, R., Amaral, D., Bliss, T., & O'Keefe, J. (2007) The hippocampus book. Oxford University Press: Oxford.

Aoki, Y., Ishii, R., Pascual-Marqui, R. D., Canuet, L., Ikeda, S., Hata, M., et al. (2015). Detection of EEG-resting state independent networks by eLORETA-ICA method. *Frontiers in Human Neuroscience*, *9*, 31.

Apostolova, L. G., Green, A. E., Babakchanian, S., Hwang, K. S., Chou, Y. Y., Toga, A. W., et al. (2012). Hippocampal atrophy and ventricular enlargement in normal aging, mild cognitive impairment (MCI), and Alzheimer Disease. *Alzheimer Disease and Associated Disorders*, *26*, 17–27.

Babiloni, C., Vecchio, F., Mirabella, G., Buttiglione, M., Sebastiano, F., Picardi, A., et al. (2009). Hippocampal, amygdala, and neocortical synchronization of theta rhythms is related to an immediate recall during rey auditory verbal learning test. *Human Brain Mapping*, *30*, 2077–2089.

Barnes, J., Boyes, R. G., Lewis, E. B., Schott, J. M., Frost, C., Scahill, R. I., et al. (2007). Automatic calculation of hippocampal atrophy rates using a hippocampal template and the boundary shift integral. *Neurobiology of Aging*, *28*, 1657–1663.

Barry, R. J., De Blasio, F. M., & Borchard, J. P. (2014). Sequential processing in the equiprobable auditory Go/NoGo task: children vs. adults. *Clinical Neurophysiology*, *125*, 1995–2006.

Bassett, D. S. & Bullmore, E. (2006). Small-world brain networks. *The Neuroscientist*, *12*, 512–523.

Blinowska, K. J. & Kaminski, M. (2013). Functional brain networks: random, "small world" or deterministic? *PloS One*, *8*, e78763.

Bobinski, M., de Leon, M. J., Wegiel, J., Desanti, S., Convit, A., Saint Louis, L. A., et al. (2000). The histological validation of post mortem magnetic resonance imaging-determined hippocampal volume in Alzheimer's disease. *Neuroscience*, *95*, 721–725.

Brett, M., Johnsrude, I. S., & Owen, A. M. (2002). The problem of functional localization in the human brain. *Nature Reviews. Neuroscience*, *3*, 243–249.

Buzsaki, G. & Draguhn, A. (2004). Neuronal oscillations in cortical networks. *Science*, *304*, 1926–1929.

Canuet, L., Ishii, R., Pascual-Marqui, R. D., Iwase, M., Kurimoto, R., Aoki, Y., et al. (2011). Resting-state EEG source localization and functional connectivity in schizophrenia-like psychosis of epilepsy. *PloS One*, *6*, e27863.

Carlesimo, G. A., Caltagirone, C., & Gainotti, G. (1996). The Mental Deterioration Battery: normative data, diagnostic reliability and qualitative analyses of cognitive impairment. The Group for the Standardization of the Mental Deterioration Battery. *European Neurology*, *36*, 378–384.

Chandler, M. J., Lacritz, L. H., Cicerello, A. R., Chapman, S. B., Honig, L. S., Weiner, M. F., et al. (2004). Three-word recall in normal aging. *Journal of Clinical and Experimental Neuropsychology*, *26*, 1128–1133.

D'Amelio, M. & Rossini, P. M. (2012). Brain excitability and connectivity of neuronal assemblies in Alzheimer's disease: from animal models to human findings. *Progress in Neurobiology*, *99*, 42–60.

Delacourte, A., David, J. P., Sergeant, N., Buee, L., Wattez, A., Vermersch, P., et al. (1999). The biochemical pathway of neurofibrillary degeneration in aging and Alzheimer's disease. *Neurology*, *52*, 1158–1165.

deToledo-Morrell, L., Stoub, T. R., Bulgakova, M., Wilson, R. S., Bennett, D. A., Leurgans, S., et al. (2004). MRI-derived entorhinal volume is a good predictor of conversion from MCI to AD. *Neurobiology of Aging*, *25*, 1197–1203.

Dierks, T., Jelic, V., Pascual-Marqui, R. D., Wahlund, L., Julin, P., Linden, D. E., et al. (2000). Spatial pattern of cerebral glucose metabolism (PET) correlates with localization of intracerebral EEG-

generators in Alzheimer's disease. *Clinical Neurophysiology*, *111*, 1817–1824.

Du, A. T., Schuff, N., Amend, D., Laakso, M. P., Hsu, Y. Y., Jagust, W. J., et al. (2001). Magnetic resonance imaging of the entorhinal cortex and hippocampus in mild cognitive impairment and Alzheimer's disease. *Journal of Neurology, Neurosurgery, and Psychiatry*, *71*, 441–447.

Dubois, B., Feldman, H. H., Jacova, C., Cummings, J. L., DeKosky, S. T., Barberger-Gateau, P., et al. (2010). Revising the definition of Alzheimer's disease: a new lexicon. *Lancet Neurology*, *9*, 1118–1127.

Dubois, B., Feldman, H. H., Jacova, C., Hampel, H., Molinuevo, J. L., Blennow, K., et al. (2014). Advancing research diagnostic criteria for Alzheimer's disease: the IWG-2 criteria. *Lancet Neurology*, *13*, 614–629.

Fox, N. C., Warrington, E. K., Freeborough, P. A., Hartikainen, P., Kennedy, A. M., Stevens, J. M., et al. (1996). Presymptomatic hippocampal atrophy in Alzheimer's disease. A longitudinal MRI study. *Brain*, *119*(Pt 6), 2001–2007.

Fox, N. C., Crum, W. R., Scahill, R. I., Stevens, J. M., Janssen, J. C., & Rossor, M. N. (2001). Imaging of onset and progression of Alzheimer's disease with voxel-compression mapping of serial magnetic resonance images. *Lancet*, *358*, 201–205.

Friston, K. J. (1994). Functional and effective connectivity in neuroimaging: A synthesis. *Human Brain Mapping*, *2*, 56–78.

Fuchs, M., Kastner, J., Wagner, M., Hawes, S., & Ebersole, J. S. (2002). A standardized boundary element method volume conductor model. *Clinical Neurophysiology*, *113*, 702–712.

Gosche, K. M., Mortimer, J. A., Smith, C. D., Markesbery, W. R., & Snowdon, D. A. (2002). Hippocampal volume as an index of Alzheimer neuropathology: findings from the Nun Study. *Neurology*, *58*, 1476–1482.

Greenblatt, R. E., Ossadtchi, A., & Pflieger, M. E. (2005). Local Linear Estimators for the Bioelectromagnetic Inverse Problem. *IEEE Transactions on Signal Processing*, *53*, 3403–3412.

Hughes, C. P., Berg, L., Danziger, W. L., Coben, L. A., & Martin, R. L. (1982). A new clinical scale for the staging of dementia. *The British Journal of Psychiatry*, *140*, 566–572.

Ikeda, S., Mizuno-Matsumoto, Y., Canuet, L., Ishii, R., Aoki, Y., Hata, M., et al. (2015). Emotion regulation of neuroticism: emotional information processing related to psychosomatic state evaluated by electroencephalography and exact low-resolution brain electromagnetic tomography. *Neuropsychobiology*, *71*, 34–41.

Iriarte, J., Urrestarazu, E., Valencia, M., Alegre, M., Malanda, A., Viteri, C., et al. (2003). Independent component analysis as a tool to eliminate artifacts in EEG: a quantitative study. *Journal of Clinical Neurophysiology*, *20*, 249–257.

Jack Jr., C. R., Petersen, R. C., Xu, Y. C., O'Brien, P. C., Smith, G. E., Ivnik, R. J., et al. (1999). Prediction of AD with MRI-based hippocampal volume in mild cognitive impairment. *Neurology*, *52*, 1397–1403.

Jack Jr., C. R., Dickson, D. W., Parisi, J. E., Xu, Y. C., Cha, R. H., O'Brien, P. C., et al. (2002). Antemortem MRI findings correlate with hippocampal neuropathology in typical aging and dementia. *Neurology*, *58*, 750–757.

Jack Jr., C. R., Bernstein, M. A., Fox, N. C., Thompson, P., Alexander, G., Harvey, D., et al. (2008). The Alzheimer's Disease Neuroimaging Initiative (ADNI): MRI methods. *Journal of Magnetic Resonance Imaging*, *27*, 685–691.

Jovicich, J., Minati, L., Marizzoni, M., Marchitelli, R., Sala-Llonch, R., Bartres-Faz, D., et al. (2015). Longitudinal reproducibility of default-mode network connectivity in healthy elderly participants: A multicentric resting-state fMRI study. *NeuroImage*, *124*, 442–454.

Jung, T. P., Makeig, S., Humphries, C., Lee, T. W., McKeown, M. J., Iragui, V., et al. (2000). Removing electroencephalographic artifacts by blind source separation. *Psychophysiology*, *37*, 163–178.

Jurcak, V., Tsuzuki, D., & Dan, I. (2007). 10/20, 10/10, and 10/5 systems revisited: their validity as relative head-surface-based positioning systems. *NeuroImage*, *34*, 1600–1611.

Kaminski, M., Blinowska, K., & Szclenberger, W. (1997). Topographic analysis of coherence and propagation of EEG activity during sleep and wakefulness. *Electroencephalography and Clinical Neurophysiology*, *102*, 216–227.

Killiany, R. J., Hyman, B. T., Gomez-Isla, T., Moss, M. B., Kikinis, R., Jolesz, F., et al. (2002). MRI measures of entorhinal cortex vs hippocampus in preclinical AD. *Neurology*, *58*, 1188–1196.

Kimura, F. (2000). Cholinergic modulation of cortical function: a hypothetical role in shifting the dynamics in cortical network. *Neuroscience Research*, *38*, 19–26.

Klimesch, W. (1996). Memory processes, brain oscillations and EEG synchronization. *International Journal of Psychophysiology*, *24*, 61–100.

Klimesch, W. (1997). EEG-alpha rhythms and memory processes. *International Journal of Psychophysiology*, *26*, 319–340.

Klimesch, W., Doppelmayr, M., Russegger, H., Pachinger, T., & Schwaiger, J. (1998). Induced alpha band power changes in the human EEG and attention. *Neuroscience Letters*, *244*, 73–76.

Lancaster, J. L., Woldorff, M. G., Parsons, L. M., Liotti, M., Freitas, C. S., Rainey, L., et al. (2000). Automated Talairach atlas labels for functional brain mapping. *Human Brain Mapping*, *10*, 120–131.

Lawton, M. P. & Brody, E. M. (1969). Assessment of older people: self-maintaining and instrumental activities of daily living. *Gerontologist*, *9*, 179–186.

Marizzoni, M., Antelmi, L., Bosch, B., Bartres-Faz, D., Muller, B. W., Wiltfang, J., et al. (2015). Longitudinal reproducibility of automatically segmented hippocampal subfields: a multisite European 3 T study on healthy elderly. *Human Brain Mapping*, *36*, 3516–3527.

Mazziotta, J., Toga, A., Evans, A., Fox, P., Lancaster, J., Zilles, K., et al. (2001). A probabilistic atlas and reference system for the human brain: International Consortium for Brain Mapping (ICBM). *Philosophical Transactions of the Royal Society of London. Series B, Biological Sciences*, *356*(1412), 1293–1322.

McKhann, G. M., Knopman, D. S., Chertkow, H., Hyman, B. T., Jack Jr., C. R., Kawas, C. H., et al. (2011). The diagnosis of dementia due to Alzheimer's disease: recommendations from the National Institute on Aging-Alzheimer's Association workgroups on diagnostic guidelines for Alzheimer's disease. *Alzheimers Dement*, *7*, 263–269.

Miraglia, F., Vecchio, F., Bramanti, P., & Rossini, P. (2015a). EEG characteristics in "eyes open" vs "eyes closed" conditions: small world network architecture in healthy aging and age-related brain degeneration. *Clinical Neurophysiology*, *127*, 1261–1268.

Miraglia, F., Vecchio, F., Bramanti, P., & Rossini, P. (2015b). Small-worldness characteristics and its gender relation in specific hemispheric networks. *Neuroscience*, *310*, 1–11.

Mobascher, A., Brinkmeyer, J., Warbrick, T., Musso, F., Wittsack, H. J., Stoermer, R., et al. (2009). Fluctuations in electrodermal activity reveal variations in single trial brain responses to painful laser stimuli–a fMRI/EEG study. *NeuroImage*, *44*(3), 1081–1092.

Modrego, P. J. (2006). Predictors of conversion to dementia of probable Alzheimer type in patients with mild cognitive impairment. *Current Alzheimer Research*, *3*, 161–170.

Monaco, M., Costa, A., Caltagirone, C., & Carlesimo, G. A. (2013). Forward and backward span for verbal and visuo-spatial data: standardization and normative data from an Italian adult population. *Neurological Sciences*, *34*, 749–754.

Mulert, C., Jager, L., Schmitt, R., Bussfeld, P., Pogarell, O., Moller, H. J., et al. (2004). Integration of fMRI and simultaneous EEG: towards a comprehensive understanding of localization and time-course of brain activity in target detection. *NeuroImage*, *22*, 83–94.

Olbrich, S., Mulert, C., Karch, S., Trenner, M., Leicht, G., Pogarell, O., et al. (2009). EEG-vigilance and BOLD effect during simultaneous EEG/fMRI measurement. *NeuroImage*, *45*, 319–332.

Onnela, J. P., Saramaki, J., Kertesz, J., & Kaski, K. (2005). Intensity and coherence of motifs in weighted complex networks. *Physical Review. E, Statistical, Nonlinear, and Soft Matter Physics*, *71*, 065103.

Pascual-Marqui, R. D. (2002). Standardized low-resolution brain electromagnetic tomography (sLORETA): technical details. *Methods and Findings in Experimental and Clinical Pharmacology*, *24* Suppl D, 5–12.

Pascual-Marqui RD. (2007) Instantaneous and lagged measurements of linear and nonlinear dependence between groups of multivariate time series: frequency decomposition. arXiv preprint arXiv:0711 1455.

Pascual-Marqui RD. (2009) Theory of the EEG Inverse Problem. In: 2009 Artech House B, editor. Quantitative EEG Analysis: Methods and Clinical Applications., pp. 121–140.

Pascual-Marqui, R. D., Michel, C. M., & Lehmann, D. (1994). Low resolution electromagnetic tomography: a new method for localizing electrical activity in the brain. *International Journal of Psychophysiology*, *18*, 49–65.

Pitkanen, A., Laakso, M., Kalviainen, R., Partanen, K., Vainio, P., Lehtovirta, M., et al. (1996). Severity of hippocampal atrophy correlates with the prolongation of MRI T2 relaxation time in temporal lobe epilepsy but not in Alzheimer's disease. *Neurology*, *46*, 1724–1730.

Pizzagalli, D. A., Pascual-Marqui, R. D., Nitschke, J. B., Oakes, T. R., Larson, C. L., Abercrombie, H. C., et al. (2001). Anterior cingulate activity as a predictor of degree of treatment response in major depression: evidence from brain electrical tomography analysis. *The American Journal of Psychiatry*, *158*, 405–415.

Pizzagalli, D. A., Oakes, T. R., Fox, A. S., Chung, M. K., Larson, C. L., Abercrombie, H. C., et al. (2004). Functional but not structural subgenual prefrontal cortex abnormalities in melancholia. *Molecular Psychiatry*, *9*(325), 393–405.

Pohlack, S. T., Meyer, P., Cacciaglia, R., Liebscher, C., Ridder, S., & Flor, H. (2014). Bigger is better! Hippocampal volume and declarative memory performance in healthy young men. *Brain Structure & Function*, *219*, 255–267.

Ramyead, A., Kometer, M., Studerus, E., Koranyi, S., Ittig, S., Gschwandtner, U., et al. (2014). Aberrant current source-density and lagged phase synchronization of neural oscillations as markers for emerging psychosis. *Schizophrenia Bulletin*, *41*, 919–929.

Rey, A. (1968). Reattivo Della Figura Complessa. Manuale. Organizzazioni Speciali, Firenze.

Ricceri, L., Minghetti, L., Moles, A., Popoli, P., Confaloni, A., De, S. R., et al. (2004). Cognitive and neurological deficits induced by early and prolonged basal forebrain cholinergic hypofunction in rats. *Experimental Neurology*, *189*, 162–172.

Rienstra, C. M. (2013). Amyloid structures from Alzheimer's disease patients. *Structure*, *21*, 1722–1723.

Roman, G. C., Tatemichi, T. K., Erkinjuntti, T., Cummings, J. L., Masdeu, J. C., Garcia, J. H., et al. (1993). Vascular dementia: diagnostic criteria for research studies. Report of the NINDS-AIREN international workshop. *Neurology*, *43*, 250–260.

Rosen, W. G., Terry, R. D., Fuld, P. A., Katzman, R., & Peck, A. (1980). Pathological verification of ischemic score in differentiation of dementias. *Annals of Neurology*, *7*, 486–488.

Rossini, P. M., Desiato, M. T., Lavaroni, F., & Caramia, M. D. (1991). Brain excitability and electroencephalographic activation: non-invasive evaluation in healthy humans via transcranial magnetic stimulation. *Brain Research*, *567*, 111–119.

Rullmann, M., Anwander, A., Dannhauer, M., Warfield, S. K., Duffy, F. H., & Wolters, C. H. (2009). EEG source analysis of epileptiform activity using a 1 mm anisotropic hexahedra finite element head model. *NeuroImage*, *44*, 399–410.

Scheltens, P., Fox, N., Barkhof, F., & De, C. C. (2002). Structural magnetic resonance imaging in the practical assessment of dementia: beyond exclusion. *Lancet Neurology*, *1*, 13–21.

Scoville, W. B. & Milner, B. (1957). Loss of recent memory after bilateral hippocampal lesions. *Journal of Neurology, Neurosurgery, and Psychiatry*, *20*, 11–21.

Sekihara, K., Sahani, M., & Nagarajan, S. S. (2005). Localization bias and spatial resolution of adaptive and non-adaptive spatial filters for MEG source reconstruction. *NeuroImage*, *25*, 1056–1067.

Selden, N. R., Gitelman, D. R., Salamon-Murayama, N., Parrish, T. B., & Mesulam, M. M. (1998). Trajectories of cholinergic pathways within the cerebral hemispheres of the human brain. *Brain*, *121*(Pt 12), 2249–2257.

Shi, F., Liu, B., Zhou, Y., Yu, C., & Jiang, T. (2009). Hippocampal volume and asymmetry in mild cognitive impairment and Alzheimer's disease: Meta-analyses of MRI studies. *Hippocampus*, *19*, 1055–1064.

Sporns, O. & Honey, C. J. (2006). Small worlds inside big brains. *Proceedings of the National Academy of Sciences of the United States of America*, *103*, 19219–19220.

Stam, C. J., Jones, B. F., Nolte, G., Breakspear, M., & Scheltens, P. (2007). Small-world networks and functional connectivity in Alzheimer's disease. *Cerebral Cortex*, *17*, 92–99.

Stam, C. J., de Haan, W., Daffertshofer, A., BF, J., Manshanden, I., van Walsum AM, v. C., et al. (2009). Graph theoretical analysis of magnetoencephalographic functional connectivity in Alzheimer's disease. *Brain*, *132*, 213–224.

Steriade, M. & Llinas, R. R. (1988). The functional states of the thalamus and the associated neuronal interplay. *Physiological Reviews*, *68*, 649–742.

Tanaka, Y., Hanyu, H., Sakurai, H., Takasaki, M., & Abe, K. (2003). Atrophy of the substantia innominata on magnetic resonance imaging predicts response to donepezil treatment in Alzheimer's disease patients. *Dementia and Geriatric Cognitive Disorders*, *16*, 119–125.

Teipel, S. J., Flatz, W. H., Heinsen, H., Bokde, A. L., Schoenberg, S. O., Stockel, S., et al. (2005). Measurement of basal forebrain atrophy in Alzheimer's disease using MRI. *Brain*, *128*, 2626–2644.

Van, P. C. (2004). Relationship between hippocampal volume and memory ability in healthy individuals across the lifespan: review and meta-analysis. *Neuropsychologia*, *42*, 1394–1413.

van der Flier, W. M., van Straaten, E. C., Barkhof, F., Ferro, J. M., Pantoni, L., Basile, A. M., et al. (2005). Medial temporal lobe atrophy and white matter hyperintensities are associated with mild cognitive deficits in non-disabled elderly people: the LADIS study. *Journal of Neurology, Neurosurgery, and Psychiatry*, *76*, 1497–1500.

Vecchio, F., Babiloni, C., Lizio, R., Fallani, F. V., Blinowska, K., Verrienti, G., et al. (2013). Resting state cortical EEG rhythms in Alzheimer's disease: toward EEG markers for clinical applications: a review. *Supplements to Clinical Neurophysiology*, *62*, 223–236.

Vecchio, F., Miraglia, F., Bramanti, P., & Rossini, P. M. (2014a). Human brain networks in physiological aging: a graph theoretical analysis of cortical connectivity from EEG data. *Journal of Alzheimer's Disease*, *41*, 1239–1249.

Vecchio, F., Miraglia, F., Marra, C., Quaranta, D., Vita, M. G., Bramanti, P., et al. (2014b). Human brain networks in cognitive decline: a graph theoretical analysis of cortical connectivity from EEG data. *Journal of Alzheimer's Disease*, *41*, 113–127.

Vecchio, F., Miraglia, F., Valeriani, L., Scarpellini. MG., Bramanti, P., Mecarelli, O., Rossini, PM. (2014c) Cortical brain connectivity and b-type natriuretic peptide in patients with congestive heart failure. *Clinical EEG and Neuroscience*.

Vecchio, F., Miraglia, F., Curcio, G., Altavilla, R., Scrascia, F., Giambattistelli, F., et al. (2015a). Cortical brain connectivity evaluated by graph theory in dementia: a correlation study between functional and structural data. *Journal of Alzheimer's Disease*, *45*(3), 745–756.

Vecchio, F., Miraglia, F., Valeriani, L., Scarpellini, M. G., Bramanti, P., Mecarelli, O., et al. (2015b). Cortical brain connectivity and b-type

natriuretic peptide in patients with congestive heart failure. *Clinical EEG and Neuroscience*, *46*, 224–229.

Vecchio, F., Miraglia, F., Quaranta, D., Granata, G., Romanello, R., Marra, C., Bramanti, P., Rossini, PM. (2016) Cortical connectivity and memory performance in cognitive decline: a study via graph theory from EEG data. *Neuroscience*, *316*, 143–50.

Vitacco, D., Brandeis, D., Pascual-Marqui, R., & Martin, E. (2002). Correspondence of event-related potential tomography and functional magnetic resonance imaging during language processing. *Human Brain Mapping*, *17*, 4–12.

Volpe, U., Mucci, A., Bucci, P., Merlotti, E., Galderisi, S., & Maj, M. (2007). The cortical generators of P3a and P3b: a LORETA study. *Brain Research Bulletin*, *73*, 220–230.

Watts, D. J. & Strogatz, S. H. (1998). Collective dynamics of 'small-world' networks. *Nature*, *393*, 440–442.

Whitwell, J. L., Crum, W. R., Watt, H. C., & Fox, N. C. (2001). Normalization of cerebral volumes by use of intracranial volume: implications for longitudinal quantitative MR imaging. *AJNR. American Journal of Neuroradiology*, *22*, 1483–1489.

Wolz, R., Julkunen, V., Koikkalainen, J., Niskanen, E., Zhang, D. P., Rueckert, D., et al. (2011). Multi-method analysis of MRI images in early diagnostics of Alzheimer's disease. *PloS One*, *6*, e25446.

Worrell, G. A., Lagerlund, T. D., Sharbrough, F. W., Brinkmann, B. H., Busacker, N. E., Cicora, K. M., et al. (2000). Localization of the epileptic focus by low-resolution electromagnetic tomography in patients with a lesion demonstrated by MRI. *Brain Topography*, *12*, 273–282.

Xie, T. & He, Y. (2011). Mapping the Alzheimer's brain with connectomics. *Frontiers in Psychology*, *2*, 77.

Yesavage, J. A., Brink, T. L., Rose, T. L., Lum, O., Huang, V., Adey, M., et al. (1982). Development and validation of a geriatric depression screening scale: a preliminary report. *Journal of Psychiatric Research*, *17*, 37–49.

Zimny, A., Szewczyk, P., Trypka, E., Wojtynska, R., Noga, L., Leszek, J., et al. (2011). Multimodal imaging in diagnosis of Alzheimer's disease and amnestic mild cognitive impairment: value of magnetic resonance spectroscopy, perfusion, and diffusion tensor imaging of the posterior cingulate region. *Journal of Alzheimer's Disease*, *27*, 591–601.

Zumsteg, D., Wennberg, R. A., Treyer, V., Buck, A., & Wieser, H. G. (2005). H2(15)O or 13NH3 PET and electromagnetic tomography (LORETA) during partial status epilepticus. *Neurology*, *65*, 1657–1660.

Zumsteg, D., Friedman, A., Wieser, H. G., & Wennberg, R. A. (2006a). Propagation of interictal discharges in temporal lobe epilepsy: correlation of spatiotemporal mapping with intracranial foramen ovale electrode recordings. *Clinical Neurophysiology*, *117*, 2615–2626.

Zumsteg, D., Lozano, A. M., & Wennberg, R. A. (2006b). Depth electrode recorded cerebral responses with deep brain stimulation of the anterior thalamus for epilepsy. *Clinical Neurophysiology*, *117*, 1602–1609.

Zumsteg, D., Lozano, A. M., Wieser, H. G., & Wennberg, R. A. (2006c). Cortical activation with deep brain stimulation of the anterior thalamus for epilepsy. *Clinical Neurophysiology*, *117*, 192–207.